J|A|C|S
JOURNAL OF THE AMERICAN CHEMICAL SOCIETY

Article

pubs.acs.org/JACS

Enhancement of SERS Background through Charge Transfer Resonances on Single Crystal Gold Surfaces of Various Orientations

Katsuyoshi Ikeda,*[†,‡,§] Shuto Suzuki,[†] and Kohei Uosaki[†,§,⊥]

[†]Division of Chemistry, Graduate School of Science, Hokkaido University, Sapporo 060-0810, Japan

[‡]Japan Science and Technology Agency, PRESTO, 4-1-8 Honcho, Kawaguchi, Saitama 332-0012, Japan

[§]Global Research Center for Environment and Energy Based on Nanomaterials Science (GREEN), National Institute for Materials Science (NIMS), Tsukuba 305-0044, Japan

[⊥]International Center for Materials Nanoarchitectonics (WPI-MANA), National Institute for Materials Science (NIMS), Tsukuba 305-0044, Japan

Supporting Information

ABSTRACT: Surface-enhanced Raman scattering (SERS) spectra are accompanied by broad background emission, which limits improvements in the signal-to-noise ratio. Despite the close correlation between the background generation and the SERS enhancement, the chemical origin of the background emission has remained somewhat mysterious. In this work, SERS spectra of organic monolayers are systematically measured on an atomically defined single crystalline gold surface of various orientations, which specifically define metal—molecule chemical interactions. The use of sphere—plane type plasmonic nanogap structures on a well-defined surface enables us to evaluate the contribution of charge transfer resonances to SERS enhancement. The present results not only reveal that charge transfer resonance at metal—molecule interfaces increases the intensity of plasmon-mediated broadband emission but also provide us a consistent view about electronic structures of metal—molecule interfaces.

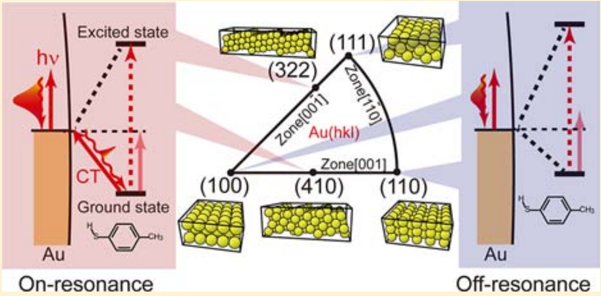

INTRODUCTION

Since the discovery of surface-enhanced Raman scattering (SERS) in the 1970s,[1,2] it has been frequently pointed out that a broad background emission is generated in conjunction with the SERS effect.[3−7] In SERS spectra, vibrational Raman peaks are always superimposed on a broad background. The intensity of the background emission is closely related to the SERS enhancement, suggesting that the background generation is intimately connected to the origin of SERS. Nevertheless, the mechanism of this phenomenon remains poorly understood; Fleishmann et al. have aptly mentioned that the appearance of a broad background was one of the experimental anomalies in SERS.[8] Actually, when SERS is exploited in practical analyses, the background continuum is simply neglected in most cases. However, the SERS background limits improvements in the signal-to-noise ratio of SERS spectra because of the relation between the enhanced Raman peaks and the enhanced broad background. Therefore, a deeper understanding of the background generation is necessary for further development of SERS spectroscopy.

It is widely recognized that there are two possible mechanisms for SERS enhancement: electromagnetic (EM) and chemical (CM) effects.[9−12] The former, which is the major source of the SERS enhancement, is caused by local field enhancement under excitation of surface plasmons on metal nanostructures.[13,14] The latter is due to charge transfer resonances between metal states near the Fermi level and a molecular electronic state.[15] To gain signal intensity from the EM effect, conventional SERS spectroscopy is conducted on a plasmonic substrate with a nanostructured surface, such as electrochemically roughened metal surfaces or metal nanoparticle aggregates. However, the poorly controlled morphology of such substrates causes a serious problem for controlling the degrees of both EM and CM, resulting in difficulty in systematic understanding of the background generation in SERS.

In the past decade, SERS spectroscopy has benefited from significant advancements in nanofabrication technology. EM is now controllable through fabrication of well-shaped plasmonic nanostructures.[16−21] Accordingly, several reports on well-designed SERS experiments have revealed that spectral appearance of the SERS background is clearly dependent on plasmon resonance features of SERS-active substrates. This indicates a close correlation between background generation and the EM effect.[7,22,23] On the other hand, except for the electrochemical method, CM is not controllable because of undefined metal—molecule interactions on a nanostructured

Received: July 20, 2013
Published: October 25, 2013

dx.doi.org/10.1021/ja407459t | *J. Am. Chem. Soc.* 2013, 135, 17387−17392

metal surface with various adsorption sites exposed. Therefore, the CM contribution to the SERS background remains unclear from experimental viewpoints, even though a number of electrochemical SERS studies have suggested a close correlation.[8,12,15]

We have recently reported that both EM and CM contributions to SERS spectra can be well-managed when SERS observations are conducted on a single crystal metal surface with well-defined atomic arrangements.[24] Chemical interactions at the substrate-molecule interface can be varied by alternating the crystallographic orientation of the metal substrate. Although plasmon excitation is normally forbidden on such a planar surface, one can leverage excitation of highly localized plasmon modes on it through the application of sphere–plane type plasmonic nanogap structures, which can be formed by deposition of gold nanoparticles (Au-NPs) on a chemically modified metal substrate[24−30] or of shell-isolated Au-NPs on a metal surface.[31−33] In this work, SERS spectra of self-assembled organic monolayers (SAMs) are systematically studied on single crystal gold substrates of various orientations. The close relation between the background generation and SERS enhancement is evident from our results, suggesting that charge transfer resonances at metal–molecule interfaces enhance background emission as well as Raman bands in SERS spectra.

■ RESULTS AND DISCUSSION

Figure 1 shows a sphere–plane type plasmonic nanogap structure, which is the key for SERS observations on atomically planar metal surfaces. Five different orientations of the Au substrate were utilized in the present SERS experiments to examine the contribution of the difference of the substrate–molecule interfaces to SERS spectra: low index faces of Au(111), Au(100), and Au(110) and high index faces of Au(322) = $5(111)_{\text{terrace}}-(100)_{\text{step}}$ and Au(410) = $4(100)_{\text{terrace}}-(110)_{\text{step}}$. The crystallographic relations among these orientations are illustrated in the bottom panel of Figure 1.

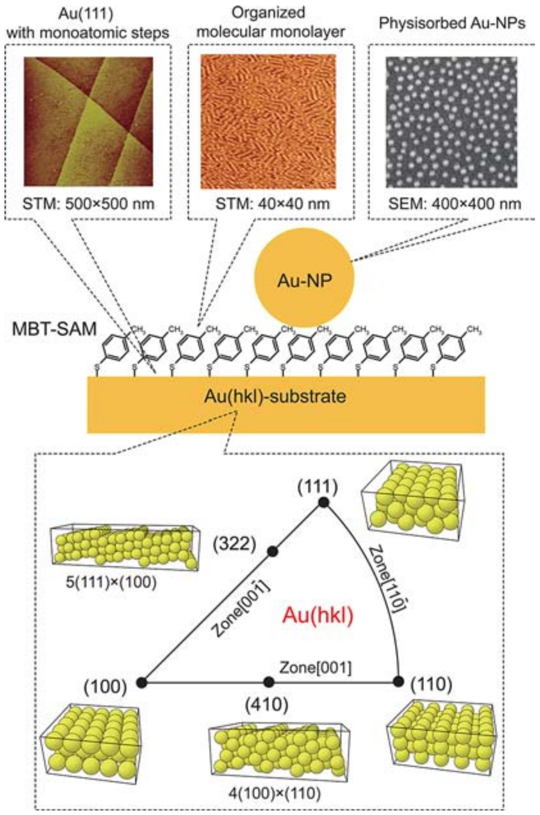

Figure 1. Schematic illustration of the Au-NPs/MBT-SAM/Au(*hkl*) system. Top left panel: a typical STM image of the Au(111) substrate, indicating the atomically defined surface. Top middle panel: the molecular-resolved STM image of MBT-SAMs. Top right panel: the SEM image of Au-NPs physisorbed on top of the SAM. The bottom panel: stereographic triangle for a face-centered cubic (fcc) gold single crystal showing the relation between the crystallographic orientations, (111), (100), (110), (322), and (410).

These surfaces were modified with SAMs of 4-methylbenzenethiol (MBT). Au-NPs with a diameter of 20 nm ±2.0 nm (purchased from Tanaka precious metals) were then electrostatically deposited on top of the SAM. The top left panel in Figure 1 shows a typical STM image of Au(111): wide triangular terraces and monatomic steps are formed, indicating that the obtained surface is indeed atomically defined. The top middle panel shows a molecularly resolved STM image of MBT-SAMs on Au(111), showing that the adsorbed molecules are two-dimensionally ordered. The surface density of the SAMs on each crystal face was determined by the reductive desorption method. Au-NPs adsorbed on the organic layer were confirmed with SEM, as seen in the micrograph shown in the top right panel of Figure 1. Typical coverage of the deposited Au-NPs was around 30% and did not depend on the crystallographic orientation. In the present SERS system, field enhancement occurs within the sphere–plane gap,[34−36] meaning that one can estimate the density of SERS hot spots from SEM photographs of adsorbed Au-NPs. Since the optical constants for Au are independent of crystallographic orientation (see Supporting Information Figure S2), the magnitude of EM enhancement is determined by the gap distance, which in the present case is equal to the SAM thickness.[24−30,37,38] Accordingly, the measured SERS spectra can be normalized in intensity by considering the densities of SAMs and Au-NPs, leading to quantitative comparison of their signal enhancement. We have confirmed that the molecule–substrate interfaces remain intact in the presence of Au-NPs; transfer of molecules from the substrate surface to Au-NP surfaces was negligible during the SERS experiments (see Supporting Information Figure S4).

SERS observations of Au-NPs/MBT-SAM/Au(*hkl*) were conducted using He–Ne laser radiation of 632.8 nm (1.96 eV). Figure 2 shows the sphere–plane nanogap induced SERS spectra measured on the five different substrate orientations. The normalized SERS intensity for (111), (100), and (110) orientations were very similar, indicating that the SERS enhancement was almost the same on these surfaces. The spectral features were also very similar on these surfaces; only Raman-active a1 modes appeared in the spectra.[24,39−41] The peak assignments are summarized in Table 1. As for the SERS background, no apparent feature was found on these surfaces. In contrast, the Au(322) and (410) surfaces showed relatively high SERS enhancement. For example, the 1078 cm^{-1} peak (νCS, a1) on Au(410) was 2.5 times larger than that on Au(111). Moreover, additional peaks were found at 1298, 1446, and 1541 cm^{-1}, which were assigned to the originally Raman-forbidden nontotally symmetric b2 modes.[24,39−41] Activation of such modes is generally induced by charge transfer resonances at the metal–molecule interface, that is, CM contribution; therefore, the present results suggest that the CM contribution is larger for (322) and (410) than for other faces. We also

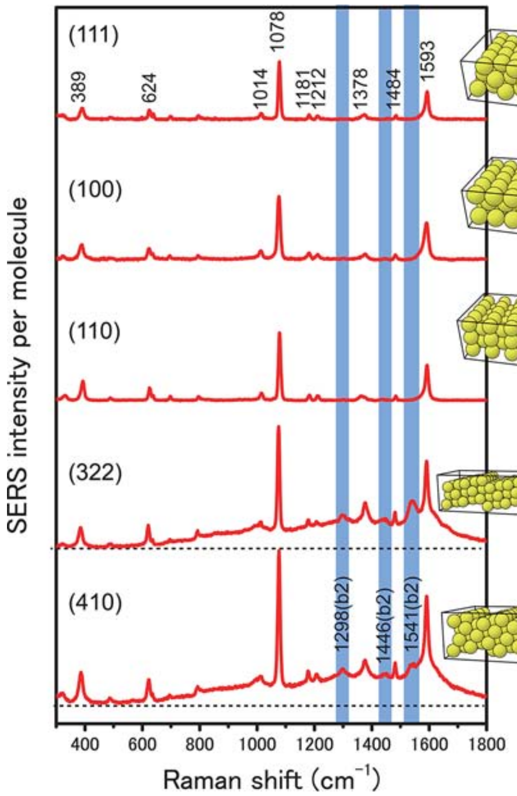

Figure 2. Sphere−plane nanogap-induced SERS spectra of MBT-SAMs measured for the (111), (100), (110), (322), and (410) surface orientations under ambient conditions. The signal intensity for each spectrum is normalized with respect to the density of MBTs. The (322) and (410) surfaces exhibited stronger SERS intensity along with significantly larger background continuum generation.

Table 1. Raman Band Frequencies (cm^{-1}) of MBT

Au(111)	Au(322)	assignments[a]
389	392	νCS + γCCC, 6a(a1)
624	621	γCCC, 12(a1)
1014	1013	γCC + γCCC, 18a(a1)
1078	1075	νCS, 7a(a1)
1181	1177	δCH, 9a(a1)
1212	1206	νCCH$_3$ + δCH
	1298	νCC + δCH, 14(b2)
1378	1376	νCCH$_3$ + δCH$_3$
	1446	νCC + δCH, 19b(b2)
1484	1481	νCC + δCH, 19a(a1)
	1541	νCC, 8b(b2)
1593	1591	νCC, 8a(a1)

[a] Approximate description of the modes (ν, stretch; δ and γ, bend). For ring vibrations, the corresponding vibrational modes of benzene and the symmetry species under $C_{2\nu}$ symmetry are indicated.

noticed that these two surfaces revealed a relatively large background in the range between 600 and 1800 cm^{-1}. This strongly indicates that the larger SERS enhancement is accompanied by larger background, as several researchers have pointed out in conventional SERS studies using a rough metal surface.

The close relation between the background and CM can be confirmed by electrochemical SERS observations in the sphere−plane system. Although the electrochemical SERS measurement is a common technique in conventional SERS spectroscopy for a roughened metal surface, there are few reports for a single crystal surface.[24,31−33] The electrochemical tuning of the Fermi level of gold can influence the resonance condition of metal−molecule charge transfers through variation of the energy difference between metal states and molecular energy levels. Figure 3a shows the electrochemical potential dependence of the SERS spectra of MBT-SAMs on Au(322). Both the SERS intensity and background were reversibly varied under the potential sweep between 0 and 0.8 V vs Ag/AgCl. Although the potential tuning may affect the molecular orientations, this possibility is negligible in the present potential region because the relative peak intensities of the a1 modes did not show any change. The observed behavior is summarized in Figure 3b: the intensity variations of 7a(a1) at 1078 cm^{-1} and 8b(b2) at 1541 cm^{-1} are plotted as a function of the electrode potential as well as the background intensity at 1250 cm^{-1}. Both the a1 and b2 modes show very similar potential dependence with a maximum at around 0.3 V. Such a potential dependence is recognized to be characteristic in the electronic resonance.[12] More importantly, the background intensity

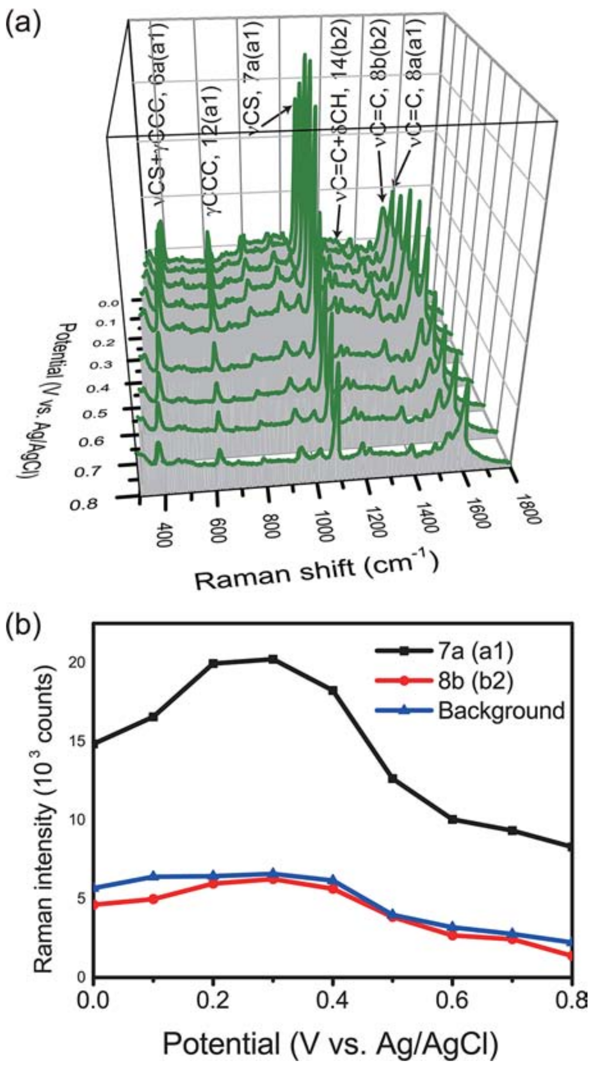

Figure 3. (a) Electrochemical potential dependence of the sphere−plane nanogap-induced SERS spectra of MBT-SAMs on Au(322). (b) Intensity variations of 7a, 8b, and the background as a function of the applied potential.

synchronously changed with the potential profiles of the SERS peaks. This confirms that the background emission process is influenced by the CM effect.

The crystallographic orientation dependence of CM is not due to high-index faces alone, but rather, is due to the combination of molecules and crystal orientation. We have previously reported another example of crystallographic orientation dependence of SERS spectra in 4-aminobenzenethiols (ABT, or sometimes abbreviated as pATP) on low-index faces of gold.[24] In contrast with MBT, the CM contribution for ABT was found to be larger for Au(111) than for Au(100). The larger background was accompanied by a larger SERS intensity on Au(111) even in this case, although we did not discuss it in the previous report. Moreover, we have confirmed that SERS spectrum of ABT on high-index faces is rather similar to that on Au(100) having the weaker CM resonance features, as shown in Supporting Information Figure S5.

The SERS enhancement factor, EF, as the ratio of the Raman scattered peak intensity in the presence of the metal substrate to its value in the absence of the metal can be defined as follows:[12,13]

$$\mathrm{EF} = |\alpha_{\mathrm{R}}/\alpha_{\mathrm{R0}}|^2 |g(\omega_{\mathrm{sc}})\, g(\omega_{\mathrm{i}})|^2 \qquad (1)$$

Here, the EM effect refers to the $|g(\omega_{\mathrm{sc}})\, g(\omega_{\mathrm{i}})|^2$ term, where $g(\omega)$ is the local field enhancement on a metal surface as a function of frequency, ω, and ω_{sc} and ω_{i} indicate frequency of scattered light and incident light, respectively. α_{R} and α_{R0} are Raman polarizabilities of the adsorbed and isolated molecules, respectively. Since $g(\omega)$ is characterized by plasmon resonances of the metal nanostructures, the EM contribution to SERS conforms well to the plasmon resonances. In the present experiments, this effect is well controlled by the use of the sphere–plane nanogap structures (see Supporting Information Figure S3).[24−30,37,38] On the other hand, the CM effect is incorporated in the $|\alpha_{\mathrm{R}}/\alpha_{\mathrm{R0}}|^2$ term. In a metal–molecule system, α_{R} may be greatly altered in its resonant property from α_{R0} when metal-to-molecule or molecule-to-metal charge transfer occurs. According to the theoretical treatment for resonance Raman scattering, the Raman polarizability in a metal–molecule system can be written as

$$\alpha_{\mathrm{R}} = A + B + C \qquad (2)$$

(see ref 15). The *A* term represents a Franck–Condon contribution, which can enhance only the totally symmetric modes. The *B* and *C* terms describe Herzberg–Teller contributions from molecule-to-metal and metal-to-molecule charge transfers, respectively. These vibronic terms of *B* and *C* can increase both totally and nontotally symmetric modes. Therefore, the potential dependence of the b2 modes is generally recognized as evidence for the contribution of charge transfer resonances in SERS.

For the SERS background, there is a broad consensus on the contribution of both EM and CM mechanisms. Especially, the EM contribution is well-recognized because the wavelength dependence of the background is known to well reflect the plasmonic resonance feature of SERS-active substrates.[7,22,23] The mechanism of EM-induced background generation is accounted for by intraband transitions in the sp-conduction band of gold, which is mediated by plasmonic local fields.[42] Such a direct intraband transition is normally electric-dipole-forbidden because the initial and final electronic states have the same symmetry, and these states are separated by momentum. On a SERS-active substrate, however, the optical field is plasmonically confined beyond the diffraction limit, resulting in a large wavenumber of the field that can compensate the large momentum difference for the intraband transitions; the SERS background emission is intrinsically connected to the EM contribution.

In contrast, a comprehensive explanation for the CM contribution to the background emission has not been provided, despite the several models proposed.[5,7] Recently, Lombardi et al. derived a modified expression of the Herzberg–Teller type charge transfer resonance, in which coupling of discrete molecular HOMO and LUMO levels to the metal electronic continuum states in both the filled and unfilled levels was taken into account.[43] This theory, based on the Fano interference effect,[44] explains the electrochemical potential behavior of SERS peak intensity well. In the present results, the SERS intensity for both the vibrational peaks and the background of MBT-SAM showed asymmetric line shapes with respect to the electrode potential sweep, as shown in Figure 3b, which is a characteristic feature of Fano interference. A similar Fano-like behavior has been also observed in our previous study of ABT (see Supporting Information Figure S6).[24] The synchronous behavior of the background with the vibrational peaks clearly indicates that the SERS background gains intensity from the CM effect. Note that the CM contribution alone cannot generate the background emission because of the small transition probability; the CM-induced background must gain intensity from the plasmonic effect.

The direction of the charge transfer in the CM contribution can be determined by asymmetric shape of the Fano resonance in electrochemical SERS; the asymmetry of Fano interference is sensitive to the phase difference between the Au intraband transition and CT, which is directly related to the CT direction. For ABT, the direction is known to be from metal to molecule (*C* term).[39,40] Since the asymmetry for MBT (Figure 3b) was opposite that for ABT (Supporting Information Figure S6), the charge transfer direction for MBT is attributed to be from molecule to metal (B term). This difference is ascribed to the para-substituent effect in benzenethiol derivatives; the HOMO–LUMO gap of MBT is larger than that of ABT, and the molecular dipole of MBT is smaller than that of ABT (see Supporting Information Figure S7).[41]

The degree of the CM effect under a specific energy excitation is influenced by the energy difference between the Fermi level of Au and the molecular electronic state. Although electrochemical SERS can tune the degree of the CM through variation of the Fermi level, the crystallographic orientation dependence (Figure 2) can be explained by the interfacial dipole effect between Au and the molecules, as shown in Figure 4. When the molecules are adsorbed on a metal surface, the molecular electronic levels relative to the Fermi level are shifted by the Au–S bond dipole, which incorporates both the reduction of the intrinsic surface dipole of the metal and the local charge redistribution due to bond formation.[45] The magnitude of the Au–S bond dipole is influenced by various factors, such as surface densities of thiols, molecular orientations, and atomic surface arrangements of the substrate. Since all of these factors are affected by the crystal orientation of the substrate, the degree of CM in SERS depends on the crystal orientation.

■ CONCLUSIONS

SERS spectra were measured under the control of both EM and CM contributions using the sphere–plane type plasmonic

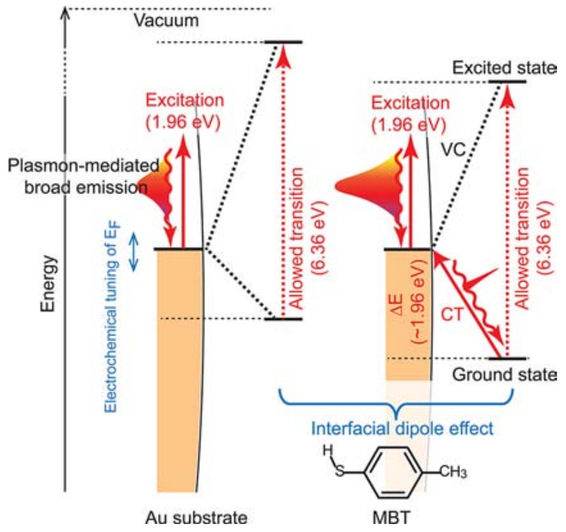

Figure 4. Schematic illustration of plasmon-mediated intraband transition in the sp band of Au and CM enhancement of the emission for the MBT/Au. CT and VC denote charge transfer resonance and vibronic coupling, respectively. The CM contribution is influenced by both the electrochemical potential and Au-MBT interfacial dipoles.

nanostructures on single crystalline gold electrodes of various orientations. The SERS background, mediated by plasmon resonances, was significantly enhanced through charge transfer resonance at the metal−molecule interfaces. Although the contribution of CM has been noted from the result of various electrochemical SERS studies on a rough surface, the precise management of metal−molecule interfaces revealed that this effect was quite sensitive to the metal−molecule interfaces. Well-controlled SERS measurements can extract not only vibrational but also electronic information from the intensities of both the Raman bands and the background. This means that SERS spectroscopy can be a powerful tool for studying metal−molecule interactions, as expected since the discovery of SERS, on a well-defined surface. To increase the signal-to-noise ratio in SERS spectroscopy, the CM-induced background should be avoided because the EM-induced background is intrinsically unavoidable in SERS. To reduce the EM-induced background, the field localization at each SERS hot spot should be carefully managed; excess field localization must be avoided. Therefore, the use of a well-defined SERS system, such as the sphere−plane structure in the present study, is better than conventional SERS substrates.

■ METHODS

Au Single Crystalline Substrates. A single crystalline gold surface having a specific orientation, Au(*hkl*), was obtained using the Clavilier method.[46] The end of a 0.8-mm diameter high-purity (99.999%) gold wire was melted and cooled slowly to generate a single crystalline Au bead. The bead was then cut along the required crystal plane and polished to a mirror finish. A clean and well-defined surface was obtained by flame-annealing and protected by a hydrogen-saturated pure water droplet. As shown in Figure 1b, Au(111), Au(100), Au(110), Au(322), and Au(410) correspond to three corners and two edges of the crystallographic triangle, respectively.[47] The rest of the edges were not examined here because of the similarity to Au(110), which consists of $(111)_{\text{terrace}}$ and $(111)_{\text{step}}$. The orientation of the prepared surfaces was checked by measuring the electrochemical behavior in a 50 mM H_2SO_4 solution (Supporting Information Figure S1).[48,49]

Molecular Monolayer. MBT-SAMs were prepared by immersion of the substrate in an ethanoic solution containing 1 mM MBT. The surface density of MBT-SAMs was estimated to be 6.3×10^{-10} mol cm^{-2} on Au(111), 5.8×10^{-10} mol cm^{-2} on Au(100), 8.9×10^{-10} mol cm^{-2} on Au(110), 5.8×10^{-10} mol cm^{-2} on Au(322), and 4.7×10^{-10} mol cm^{-2} on Au(410) by the electrochemical reductive desorption method.[50] The measured charges were corrected for capacitive charging to determine the surface densities accurately. The surface density estimated on Au(111) is in good agreement with the value expected from the previously proposed unit cell of MBT-SAMs.[51] All SERS spectra were normalized by these values. For ABT-SAMs, we have previously reported SERS spectra on Au(111) and Au(100),[24] and also measured them on Au(410). The energy gap between the HOMO and the LUMO of 4-MBT and 4-ABT was reported to be 6.36 and 5.52 eV, respectively, according to the DFT calculation.[41]

SERS Measurements. SERS observations were conducted under both ambient and electrochemical conditions using a home-built inverted Raman microscope system with an objective lens (40×, 0.6 N.A.).[24] A He−Ne laser (632.8-nm radiation with intensity of 0.02 mW) was utilized as the light source for excitation of the gap-mode plasmons. Backscattered Raman signals from the SAM-covered Au(*hkl*) substrate were monitored by a CCD-polychromator system (PIXIS 400B, Princeton Instruments) after Rayleigh scattering light was filtered by an edge filter (LP02-633-RU, Semrock). In electrochemical SERS observations, the substrate potential was controlled in a glass cell filled with Ar-bubbled 0.1 M $NaClO_4$ aqueous solution. An Ag/AgCl electrode was utilized as a reference.

■ ASSOCIATED CONTENT

Ⓢ Supporting Information

Cyclic voltammograms of Au of various orientations; crystal orientation dependence of optical constants of Au; reflection spectra of Au-NPs/MBT/Au; SERS spectrum of Au-NPs/ABT/Pt(100); normalized SERS spectra of Au-NPs/ABT/Au of (111), (100), and (410); electrochemical potential dependence of SERS spectra of Au-NPs/ABT/Au(111); and energy diagram for charge transfers at ABT/Au and MBT/Au interfaces. This material is available free of charge via the Internet at http://pubs.acs.org.

■ AUTHOR INFORMATION

Corresponding Author

E-mail: kikeda@pchem.sci.hokudai.ac.jp

Notes

The authors declare no competing financial interest.

■ ACKNOWLEDGMENTS

This research was supported in part a by Grant-in-Aid for Young Scientists (A) (No. 24681018) and that for Exploratory Research (No. 24651126) from JSPS, World Premier International Research Center (WPI) Initiative on Materials Nanoarchitechtonics and MEXT Program for Development of Environmental Technology using Nanotechnology from the Ministry of Education, Culture, Sports, Science and Technology (MEXT), Japan. SEM measurements were supported by Hokkaido Innovation through NanoTechnology Support (HINTS, Nanotechnology Network Project supported by MEXT, Japan). We also greatly acknowledge Dr. S. Yasuda and Mr. A. Furuya (Hokkaido University) for the STM measurement.

■ REFERENCES

(1) Fleischmann, M.; Hendra, P. J.; McQuillan, A. J. *Chem. Phys. Lett.* **1974**, *26*, 63.

(2) Jeanmaire, D. L.; Van Duyne, R. P. *J. Electroanal. Chem.* **1977**, *84*, 1.

(3) Gersten, J. I.; Birke, R. L.; Lombardi, J. R. *Phys. Rev. Lett.* **1979**, *43*, 147.

(4) Burstein, E.; Chen, Y. J.; Chen, C. Y.; Lundquist, S.; Tosatti, E. *Solid State Commun.* **1979**, *29*, 567.

(5) Furtak, T. E.; Reyes, J. *Surf. Sci.* **1980**, *93*, 351.

(6) Nie, S. M.; Emory, S. R. *Science* **1997**, *275*, 1102.

(7) Mahajan, S.; Cole, R. M.; Speed, J. D.; Pelfrey, S. H.; Russell, A. E.; Bartlett, P. N.; Barnett, S. M.; Baumberg, J. J. *J. Phys. Chem. C* **2010**, *114*, 7242.

(8) Fleischmann, M.; Hendra, P. J.; Hill, L. R.; Pemble, M. E. *J. Electroanal. Chem.* **1981**, *117*, 243.

(9) Otto, A.; Mrozek, I.; Grabhorn, H.; Akemann, W. *J. Phys.: Condens. Matter* **1992**, *4*, 1143.

(10) Moskovits, M. *Rev. Mod. Phys.* **1985**, *57*, 783.

(11) Morton, S. M.; Silverstein, D. W.; Jensen, L. *Chem. Rev.* **2011**, *111*, 3962.

(12) Lombardi, J. R.; Birke, R. L. *J. Chem. Phys.* **2012**, *136*, 144704.

(13) Pettinger, B. *J. Chem. Phys.* **1986**, *85*, 7442.

(14) García-Vidal, F. J.; Pendry, J. B. *Phys. Rev. Lett.* **1996**, *77*, 1163.

(15) Lombardi, J. R.; Birke, R. L.; Lu, T.; Xu, J. *J. Chem. Phys.* **1986**, *84*, 4174.

(16) Jain, P. K.; Huang, W.; El-Sayed, M. A. *Nano Lett.* **2007**, *7*, 2080.

(17) Su, K.-H.; Wei, Q.-H.; Zhang, X.; Mock, J. J.; Smith, D. R.; Schultz, S. *Nano Lett.* **2003**, *3*, 1087.

(18) Yang, Y.; Schatz, G. C.; Van Duyne, R. P. *J. Chem. Phys.* **1995**, *103*, 869.

(19) Ueno, K.; Juodkazis, S.; Shibuya, T.; Yokota, Y.; Mizeikis, V.; Sasaki, K.; Misawa, H. *J. Am. Chem. Soc.* **2008**, *130*, 6928.

(20) Kang, T.; Yoon, I.; Jeon, K.-S.; Choi, W.; Lee, Y.; Seo, K.; Yoo, Y.; Park, Q.-H.; Ihee, H.; Suh, Y. D.; Kim, B. *J. Phys. Chem. C* **2009**, *113*, 7492.

(21) Yoon, I.; Kang, T.; Choi, W.; Kim, J.; Yoo, Y.; Joo, S.-W.; Park, Q.-H.; Ihee, H.; Kim, B. *J. Am. Chem. Soc.* **2009**, *131*, 758.

(22) Farcau, C.; Astilean, S. *Chem. Commun.* **2011**, *47*, 3861.

(23) Itoh, T.; Yoshida, K.; Biju, V.; Kikkawa, Y.; Ishikawa, M.; Ozaki, Y. *Phys. Rev. B* **2007**, *76*, 085405.

(24) Ikeda, K.; Suzuki, S.; Uosaki, K. *Nano Lett.* **2011**, *11*, 1716.

(25) Ikeda, K.; Fujimoto, N.; Uehara, H.; Uosaki, K. *Chem. Phys. Lett.* **2008**, *460*, 205.

(26) Ikeda, K.; Sato, J.; Uosaki, K. *J. Photochem. Photobiol. A* **2011**, *221*, 175.

(27) Ikeda, K.; Sato, J.; Fujimoto, N.; Hayazawa, N.; Kawata, S.; Uosaki, K. *J. Phys. Chem. C* **2009**, *113*, 11816.

(28) Park, W.-H.; Kim, Z. H. *Nano Lett.* **2010**, *10*, 4040.

(29) Hill, R. T.; Mock, J. J.; Urzhumov, Y.; Sebba, D. S.; Oldenburg, S. J.; Chen, S.-Y.; Lazarides, A. A.; Chilkoti, A.; Smith, D. R. *Nano Lett.* **2010**, *10*, 4150.

(30) Kim, K.; Shin, K. S. *Anal. Sci.* **2011**, *27*, 775.

(31) Li, J. F.; Huang, Y. F.; Ding, Y.; Yang, Z. L.; Li, S. B.; Zhou, Z. S.; Fan, F. R.; Zhang, W.; Zhou, Z. Y.; Wu, D. Y.; Ren, B.; Wang, Z. L.; Tian, Z. Q. *Nature* **2010**, *464*, 392.

(32) Cui, L.; Liu, B.; Vonlanthen, D.; Mayor, M.; Fu, Y.; Li, J.-F.; Wandlowski, T. *J. Am. Chem. Soc.* **2011**, *133*, 7332.

(33) Butcher, D. P.; Boulos, S. P.; Murphy, C. J.; Ambrosio, R. C.; Gewirth, A.A. J. *Phys. Chem. C* **2012**, *116*, 5128.

(34) Aravind, P. K.; Metiu, H. *J. Phys. Chem.* **1982**, *86*, 5076.

(35) Aravind, P. K.; Metiu, H. *Surf. Sci.* **1983**, *124*, 506.

(36) Nordlander, P.; Prodan, E. *Nano Lett.* **2004**, *4*, 2209.

(37) Ikeda, K.; Takahashi, K.; Masuda, T.; Uosaki, K. *Angew. Chem., Int. Ed.* **2011**, *50*, 1280.

(38) Ikeda, K.; Takahashi, K.; Masuda, T.; Kobori, H.; Kanehara, M.; Teranishi, T.; Uosaki, K. *J. Phys. Chem. C* **2012**, *116*, 20806.

(39) Osawa, M.; Matsuda, N.; Yoshii, K.; Uchida, I. *J. Phys. Chem.* **1994**, *98*, 12702.

(40) Lombardi, J. R.; Birke, R. L. *J. Phys. Chem. C* **2008**, *112*, 5605.

(41) Kim, K.; Shin, D.; Choi, J.-Y.; Kim, K. L.; Shin, K. S. *J. Phys. Chem. C* **2011**, *115*, 24960.

(42) Beversluis, M. R.; Bouhelier, A.; Novotny, L. *Phys. Rev. B* **2003**, *68*, 115433.

(43) Lombardi, J. R.; Birke, R. L. *J. Phys. Chem. C* **2010**, *114*, 7812.

(44) Fano, U. *Phys. Rev.* **1961**, *124*, 1866.

(45) Heimel, G.; Romaner, L.; Zojer, E.; Brédas, J.-L. *Nano Lett.* **2007**, *7*, 932.

(46) Clavilier, J.; Faure, R.; Guinet, G.; Durand, R. *J. Electroanal. Chem.* **1980**, *107*, 205.

(47) Lecoeur, J.; Andro, J.; Parsons, R. *Surf. Sci.* **1982**, *114*, 320.

(48) Hamelin, A. *J. Electroanal. Chem.* **1996**, *407*, 1.

(49) Hamelin, A.; Martins, A. M. *J. Electroanal. Chem.* **1996**, *407*, 13.

(50) Walczak, M. M.; Popenoe, D. D.; Deinhammer, R. S.; Lamp, B. D.; Chung, C.; Porter, M. D. *Langmuir* **1991**, *7*, 2687.

(51) Seo, K.; Borguet, E. *J. Phys. Chem. C* **2007**, *111*, 6335.